XLI CILAMCE
XLI Ibero-Latin American Congress on Computational Methods in Engineering
16-19 November, 2020 FOZ DO IGUAÇU PARANÁ - BRAZIL

The influence of modeling techniques on the numerical analysis of composite beams

L.M. Santos[1], T. Doca[1]

[1]*ENM - Department of Mechanical Engineering, Faculty of Technology, University of Brasilia*
Campus Darcy Ribeiro, 70910-900, Brasilia, DF, Brazil
doca@unb.br

Abstract. This work aims to quantify the effects of implementation choices, such as type and number of finite elements, on the modeling composite beams. The study is carried-out on a full-size finite element model of the structure, which provides a more comprehensive description of the mechanical behavior of the system when compared to the traditional push-out test. We focus on the influence of contact conditions, physical and mechanical properties, discretization aspects and boundary conditions on the correct representation of the force-displacement, local stresses and strains in the section-stud and concrete-stud interfaces. Based on the observations, the importance of nonlinear relationships is discussed and a criteria for an adequate numerical implementation of models is proposed.

Keywords: Finite Elements, Composite Beams, Numerical Implementation

1 Introduction

Composite steel-concrete systems are a viable alternative to reinforced concrete and metallic structures. According to [1] the interaction between concrete and steel elements can significantly affect structural performance under static or dynamic loading which leads to improved stiffness, strength and ductility. In addition, its ease to built also reduce construction costs.

The main function of the shear connectors is to transfer shear force through the steel-concrete interface [2]. According to [3] interactions elements capable of resisting the bending moment may also influence the system.

Therefore, the aim of this study is to propose a numerical model for the analysis composite beams. Non-linear effects such as plasticity, damage and frictional contact are considered. The implementation is carried-out in the commercial package Abaqus coupled with Fortran subroutines.

2 Problem description

The composite beam consists of a class 2 composite section as stated in [4] . The structure is simply supported by a $HEA300$ symmetric I-profile. The concrete slab has stirrups, positive and negative longitudinal steel reinforcements made of CA50 steel. It also includes stud bolt connectors made of steel S355, and support stiffeners made of steel S235. The materials employed in the three main components of the composite system are detailed in the following.

The slab has a thickness of 100mm and a width of 1400mm. The beam length is 6600mm, the length between supports being 6000mm. There are only support stiffeners 300mm away from the beam end. The spacing between the axis of the connectors is 200mm, with the end connectors being 100mm away from the beam end (distance to the axis). For more details see the model *Beam-300* given in [5] and the work of [6]. The connectors are arranged in two rows with each row of connector 80mm away from the axis of the connector to the edge of the section and have 19mm shaft diameter, 32mm head diameter and 80mm total height.

3 Materials and methods

The stress-strain relationship adopted as input for concrete is a function of the mean compressive strength, f_{cm}, and traction, f_{tm}. With regard to compression for the stress-strain curve of concrete, the expression of [7], given in Eq. (1) , was adopted. For the ascending branch of the curve, $\zeta = 0$. The parameters Λ and Ξ used to find ζ, Eq. (3), when it is considered the descending branch of the curve are given in Eq. (4). According to [8], in the absence of experimental tests, the modulus of elasticity, E_{cm}, can be obtained through Eq. (5). In this study, the descending part of the compression curve was not considered for the global numerical models. This branch was considered only in the submodels in order to implement the damage in the concrete to the compression and the traction, through the concrete damaged plasticity model (CDP) available on Abaqus.

$$\frac{\sigma_c}{f_{cm}} = \frac{\frac{E_{cm}}{E_{c1}} + (\zeta - 1)\eta^2}{1 + \Big(\frac{E_{cm}}{E_{c1}} - 2\Big)\eta + \zeta\eta^2} \tag{1}$$

$$\eta = \frac{\varepsilon_c}{\varepsilon_{c1}},\ \varepsilon_{c1} = 0.7 \cdot f_{cm}^{0.31} \tag{2}$$

$$\zeta = \Lambda\eta + \Xi\eta^2 \tag{3}$$

$$\Lambda = 1.414 - 0.848\Big(\frac{E_{cm}}{E_{c1}}\Big),\ \Xi = -0.333 + 0.241\Big(\frac{E_{cm}}{E_{c1}}\Big) \tag{4}$$

$$E_{cm} = 22\Big(\frac{f_{cm}}{10}\Big)^{0.3},\ f_{cm} = f_{ck} + 8(MPa) \tag{5}$$

The part of the diagram that corresponds to the tensile behavior of the concrete is, according to [9], presented in Eq. (8), varying according to Hooke's law in the range $(0, 0) - (\varepsilon_{t1}, f_{tm})$, and after that point there is a decreasing to $(\varepsilon_{tu}, 0)$, where ε_{tu} chosen for critical damage, $D_c = 0.5$. The average tensile strength is given by the expression of [10] through the Eq. (9).

$$0 \leq \varepsilon \leq \varepsilon_{t1}, \qquad \sigma = \varepsilon E_{cm}, \tag{6}$$

$$\epsilon_{t1} \leq \varepsilon \leq \varepsilon_{tu}, \quad \sigma_t = f_{tm}\Big(\frac{\varepsilon - \varepsilon_{tu}}{\varepsilon_{tu} - \varepsilon_{t1}}\Big)^2, \tag{7}$$

$$\varepsilon = \varepsilon_{tu}, \qquad \sigma_t = 0. \tag{8}$$

$$f_{tm} = f_{ctk0,m}\left[\frac{f_{ck}}{f_{ck0}}\right]^{\frac{2}{3}}, f_{ck0} = 10MPa; f_{ctk0,m} = 1.4 \tag{9}$$

According to [11], compression and traction damage to concrete are calculated, respectively, by Eqs. (10). Compressive damage is calculated only for the descending branch of the stress-strain curve, analogously the simplification traction damage is calculated by assuming the same stress-strain behavior.

$$d_c = \frac{f_{cm} - \sigma_c}{f_{cm}}, \varepsilon_c \geq \varepsilon_{c1} \quad d_t = \frac{f_{tm} - \sigma_t}{f_{tm}}, \varepsilon_t \geq \varepsilon_{t1} \tag{10}$$

In the CDP model, default values were adopted, except for the viscoplastic regularization coefficient. A viscoplastic regularization coefficient is chosen wherein the ratio t/μ is sufficiently high to adequately represent the results providing a savings in computation time due to the decrease of convergence problems.

The parameters used for the implementation of the CDP model are: $\boldsymbol{\psi} = 36$, $\epsilon = 0.1$, $\sigma_{b0}/\sigma_{c0} = 1,16$, $K_c = 0.667$ e $\mu = 2e^{-6}$. Once, ψ: dilation angle; ϵ: eccentricity; σ_{b0}: biaxial concrete stress (compression); σ_{c0}: uniaxial stress of the concrete (compression); μ: coefficient of viscoplastic regularization e K_c: constant.

The material behavior was adopted for the true stress-strain curve according to [12] and its definition is shown in Fig. 1(a). For "part 4", Fig. 1(a), the relationship between stresses and strains is given according to [12] and defined by Eq. 11. The main parameters for constructing the curve are given in Table 1. The curves used as input for stud and weld are shown in Fig. 1(b). The solder material was

considered to be of the same type of steel as the head stud, but with a resistance increased by 25%, as given in [12].

$$\sigma = K\left\{\varepsilon_p + \left[\frac{\sigma_{y2}}{K}\right]^{\left(\frac{1}{n}\right)} - \varepsilon_{p,y2}\right\}^n, \varepsilon_p \geq \varepsilon_{p,y2} \tag{11}$$

For the reinforcement material (stirrups and longitudinal bars) the usual $CA50$ steel, with Young's modulus $E = 210000$MPa, was adopted. The yield stress of this steel is $\sigma_y = 500$MPa, with ratio $\sigma_u/\sigma_y = 1.08$. A strain $\varepsilon_u = 0.08$ was adopted with respect to the ultimate stress and the trilinear diagram is shown in Fig. 1(b). For the section, both the web and the flanges have the same material. The idealized model of the curve used for the construction of the strain-strain curve is given in [13]. The parameters for the true stress-strain relationships be displayed in the Table 1. The Figure 1 shows the curve adopted.

Table 1. Material properties for the true stress-strain relationship of steel $S355$ ([12]) and for the true stress-strain relationship of steel $S235$ ([13]).

Properties	**S355**	**S355(+25%)**	**S235**
E(MPa)	210000	210000	210000
σ_p(MPa)	311	400	211.7
σ_y(MPa)	346.9	446.25	236.2
σ_{y2}(MPa)	355.9	457.63	243.4
σ_u(MPa)	-	-	432.6
$\varepsilon_{p,y1}$	0.004	0.004	0.004
$\varepsilon_{p,y2}$	0.015	0.015	0.0198
$\varepsilon_{p,u}$	-	-	0.1817
K(MPa)	740	925	-
n	0.166	0.166	-
$\rho(ton/mm^3)$	$7.85 \cdot 10^{-9}$	$7.85 \cdot 10^{-9}$	$7.85 \cdot 10^{-9}$

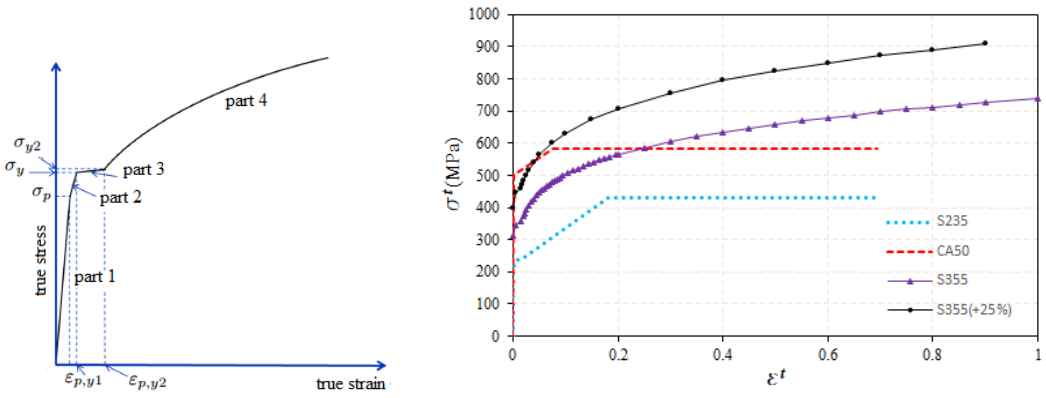

(a) Idealized true stress-strain curve([12]) (b)

Figure 1. Relation true stress *vs*. true plastic strain.

4 Implementation

This section presents the steps taken to implement the global numerical model and the sub-model. The sub-model is used to perform a more detailed analysis in the region of interest, with a more refined mesh with less computational effort.

4.1 Global model

The composite beam is modeled using a finite element-based static formulation with user defined constituitive models. Taking advantage of the symmetric nature of the structure, only a one-quarter of its geometry is required for the analysis. The loads, boundary conditions, interactions and constraints are shown in Fig. 2.

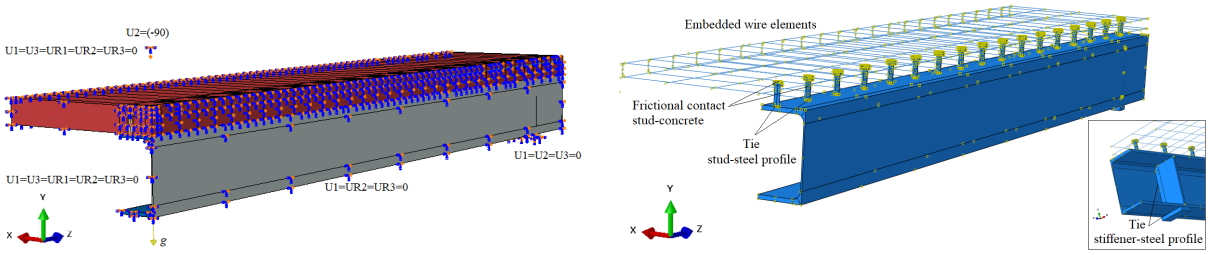

(a) Loads and boundary conditions.

(b) Interactions and constraints.

Figure 2. Global model, loads, boundary conditions, interactions and constraints.

The geometry is defined such that the Cartesian directions (x, y, z) matched the principal directions $(1, 2, 3)$. The body weight of the structure is also considered and a gravitational acceleration, g, equal to $-9810mm/s^2$ is assumed. A vertical prescribed displacement (U2) equal to $90mm$ is applied to the reference point (RP) which is kinematic coupled to an area of $50x150mm^2$ on top of the concrete slab (loading zone). The remaining degrees of freedom of the RP are fully restrained ($U1 = U3 = UR1 = UR2 = UR3 = 0$). Symmetry conditions are applied to the cross-section facet (XY plane) and the side facet (YZ plane). Restraints denoting a simply supported beam ($U1 = U2 = U3 = 0$) are also included, see Fig 2(a).

Tie constraints are applied to the connector-section and the stiffener-section interfaces. A small sliding surface-to-surface frictional contact interaction (friction coefficient of 0.7 [14]) is defined at the interface connector-concrete. The penalty method was chosen to enforce the contact constraints. Embedded wire elements are used to represent the reinforcements. The finite element mesh adopted for the global model is shown in Fig. 3.

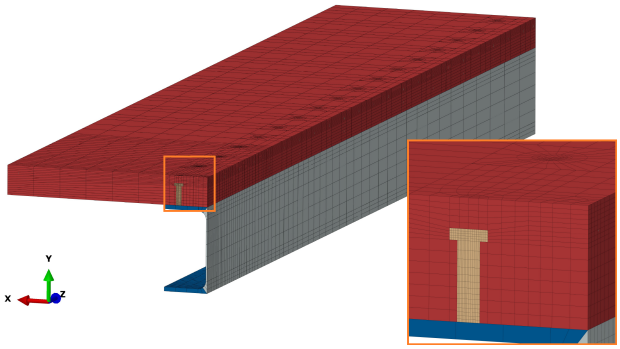

Figure 3. Discretization of the global model: Overview of the composite beam (left); and detailed view of the Profile-Stud-Concrete connection (right).

The stirrups and the longitudinal reinforcements use 2-noded linear truss elements. The decision for these specific number and types of elements were based in convergence analysis. Hexahedrical elements were used for concrete, connector, slab and stiffener, in addition to welding (in the case of the sub-model).

4.2 Submodel

Figure 4(a) displays the submodel mesh. In the submodel region there is no shear or flexural reinforcement, so only solid elements are used, and the embedded type constraint implemented in the global model is not required. In Figure 4(b) the boundary conditions of the submodel are shown, where, U_{sub}, represents the displacements imposed on the submodel due to the numerical response of the re-

spective global model. These boundary conditions reflect the node-based submodel. The interactions and constraints are presented in Fig. 4(c). Contact interfaces were used: concrete-sheet, concrete-weld, concrete-stud. Only the constraint Tie was used to simulate the constraint on the weld-plate and weld-stud interfaces.

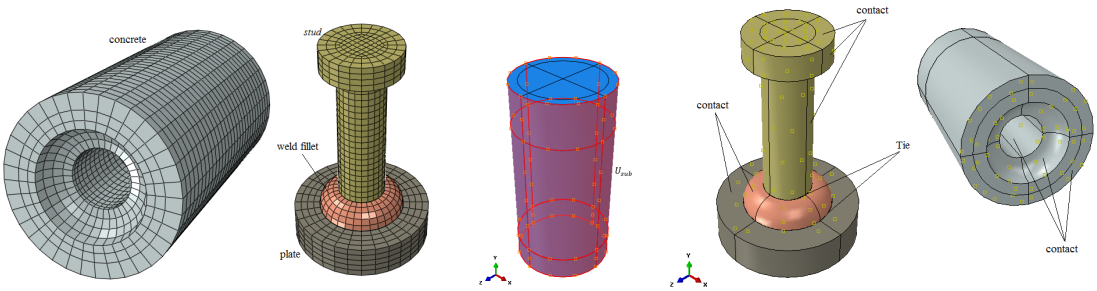

(a) Mesh (b) Boundary (c) Interactions and constraints

Figure 4. Numeric submodel

The number of finite elements for each structural element for the global and local model are presented in Tables 2 and 3, respectively. The term S2-G presented below is used to differentiate the models in relation to the discretization of the mesh and whether the analysis is global or local. In this case, "L" refers to submodels and "G" to global analysis models.

Table 2. Number of elements for global models

Instance	Size, S2-G	Tot.	Size, S3-G	Tot.	Size, S4-G	Tot.
Concrete	40	11810	60	6091	80	4531
Section	40	1411	60	715	80	369
Stud	2	9140	3	2592	4	1176

Table 3. Number of elements for the submodels

Instance	Size, S2-L	Tot.	Size, S3-L	Tot.	Size, S4-L	Tot.
Concrete	2	6308	6	1276	8	740
Section	2	1536	6	208	8	128
Stud	1	4128	3	2592	4	568
Weld	1	840	3	192	4	80

5 Results and discussion

This section presents the results for the global models and submodels with linear elements of reduced integration and full integration. As stated in the previous section, "Si-La" refer to local models with reduced integration elements, while "Si-Lb" refer to local models with full integration elements. In the case of global models, we have, in a similar way, Si-Ga and Si-Gb.

Table 4 shows the relationship between the times of the simulations, where it is possible to visualize the computational effort according to the types of elements. Among the global models there is an increase in the simulation time for models with linear elements and full integration. As for the local numerical models, partially, an inverse (and unexpected) behavior is noticed, where the greatest time is given in simulations S2-La and S3-La in relation to their peers, S2-Lb and S3-Lb, respectively . The difference, between pairs, in percentage also is shown in Table 4.

Compression and tensile damage are shown in Figs. 5(a). There is practically no difference between models with different mesh sizes for models with reduced integration elements, however between these and those with full integration there is a relevant difference of the order of 63.4%, as in the case between S2-La and S2-Lb models.

Table 4. Time differences between numerical pairs with elements of reduced and total integration.

Model	Time (s)	**Difference of time (%)**
S2-La	9553	271.57
S2-Lb	2571	
S3-La	1406	42.02
S3-Lb	990	
S4-La	251	27.67
S4-Lb	347	
S2-Ga	3333	16.63
S2-Gb	3998	
S3-Ga	1401	8.85
S3-Gb	1537	
S4-Ga	1279	8.64
S4-Gb	1279	

The plastic deformation is shown in Fig. 5(b). Different gradient values occur for the parts, that is, section, stud and weld. The greatest plastic deformation occurs in the weld, justifying the adoption of a material of higher performance for it, in relation to the welded parts.

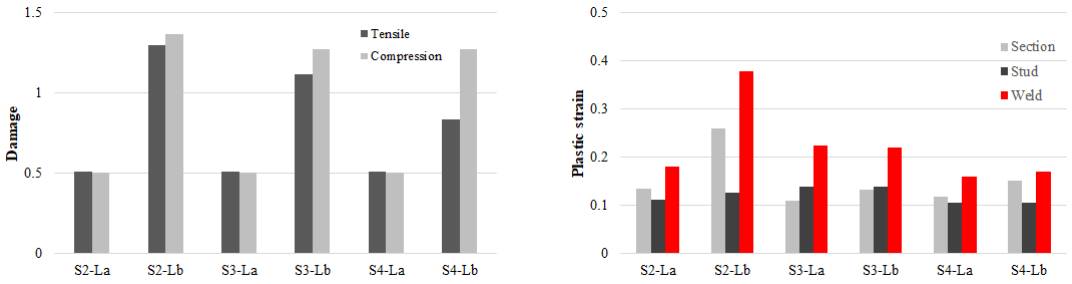

(a) Damage (b) Equivalent plastic strain

Figure 5. Outputs for submodels

For the global model, the parameter of interest for concrete was the von Mises equivalent stress, as shown in Fig. 6(a). A significant difference in this case occurred for the stress values, which were above the average maximum compression stress adopted (38MPa) for the cases with elements of total integration.

The plastic deformation in the steel elements of interest are shown in Fig. 6(b), where it is perceived that the element that deforms the most is the studs in comparison to the node with the highest gradient of equivalent plastic deformation. The differences between the maximum values between the section and the stud are, for example, 45.73% in the global model S2-Ga and 64.99% in the S2-Gb.

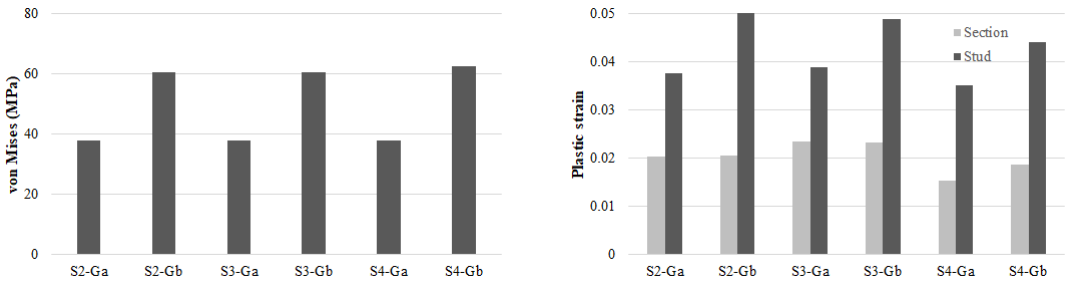

(a) von Mises stress (b) Equivalent plastic strain

Figure 6. Outputs for global models

6 Conclusions

In this work, numerical simulations were carried out to evaluate the influence of element types in the analysis of composite beams. Significant differences were noted in terms of results and computational cost. It is concluded that the models with lower computational cost can be used more frequently for analysis in mechanics of solids, in terms of number of elements, with less discretized meshes. The type of element to be adopted in a numerical simulation in a three-dimensional model must be accompanied by tests that allow its refinement in order to obtain a detailed analysis of the entire structural set.

The techniques used to implement the global numerical model and submodel were considered adequate in terms of contact, boundary conditions, mode of application of displacements, physical and geometric properties. The variables of interest analyzed, such as damage, von Mises stress and plastic strain can be seen as fundamental in the analysis of composite beams.

It is concluded that numerical evaluation methods are fundamental for the study of the mechanical behavior of composite beams of steel and concrete with ordinary materials, contributing to their understanding and identification of critical points, stress distribution, plastic strain and damage.

Acknowledgements. This work was partially supported by the Coordenação de Aperfeiçoamento de Pessoal de Nível Superior (CAPES) [Finance Code 001]. The authors gratefully acknowledge this support.

Authorship statement. The authors hereby confirm that they are the sole liable persons responsible for the authorship of this work, and that all material that has been herein included as part of the present paper is either the property (and authorship) of the authors, or has the permission of the owners to be included here.

References

[1] Cosenza, E., Sarno, L., Fabbrocino, G., & Pecce, M., 2005. Composite steel and concrete structures: Technology and design. *ACI Spring Convention 2005 Session "Seismic Engineering for Concrete Structures: Italian Perspective.*

[2] Thevendran, V., Chen, S., Shanmugam, N. E., & Richard Liew, J. Y., 1999. Nonlinear analysis of steel-concrete composite beams curved in plan. *Finite Elements in Analysis and Design*, vol. 32, n. 4, pp. 125–139.

[3] Adekola, A. O., 1968. Partial interaction between elastically connected elements of a composite beam. *Int. J. Solids Structures*, vol. 4, pp. 1125–1135.

[4] 1994-1-1, E., 2004. *Eurocode 4: Design of composite steel and concrete structures – Part 1-1: General rules and rules for buildings.* Comité Européen de Normalisation, Brussels.

[5] Hegger, J. & Döinghaus, P., 2000. High performance steel and high performance concrete in composite structures. *Composite Construction in Steel and Concrete IV.*

[6] Santos, L. M., 2019. *Análise numérica da interação mecânica de conector tipo pino com cabeça em vigas mistas.* Faculty of technology - Department of mechanical sciences (University of Brasilia), Brasilia.

[7] Sargin, M. & Handa, V., 1969. A general formulation for the stress-strain properties of concrete. , n. 3, pp. 1–27.

[8] 1992-1-1, E., 2004. *Eurocode 2: Design of concrete structures - Part 1-1: General rules and rules for buildings.* Comité Européen de Normalisation, Brussels.

[9] Grelat, A., 1978. Non-linear behavior and stability of reinforced concrete frames. *Engineering Structures*, vol. 18, n. 234, pp. 786–791.

[10] CEB/Model-Code, 1991. *CEB-FIP Model Code.* Comite Euro-International du Beton, Lausanne.

[11] Shamass, R. & Cashell, K. A., 2017. Behaviour of composite beams made using high strength steel. *Structures*, vol. 12, pp. 88–101.

[12] RP-C208, D., 2016. *Determination of structural capacity by non-linear finite element analysis methods.* Det Norske Veritas & Germanischer Lloyd, Høvik.

[13] RP-C208, D., 2013. *Determination of Structural Capacity by Non-linear FE analysis Methods.* Det Norske Veritas, Høvik.

[14] ACI-318.14, 2014. *Building Code Requirements for Structural Concrete.* American Concrete Institute, Farmington Hills.